JACS
JOURNAL OF THE AMERICAN CHEMICAL SOCIETY
Article
pubs.acs.org/JACS

Insight into the Oriented Growth of Surface-Attached Metal–Organic Frameworks: Surface Functionality, Deposition Temperature, and First Layer Order

Jin-Liang Zhuang,[†,‡,§] Martin Kind,[†] Claudia M. Grytz,[†] Frederic Farr,[†] Martin Diefenbach,[†] Samat Tussupbayev,[†] Max C. Holthausen,[†] and Andreas Terfort*[,†]

[†]Institute of Inorganic and Analytical Chemistry, University of Frankfurt, Max-von-Laue-Strasse 7, 60438 Frankfurt, Germany
[‡]School of Chemistry and Materials, Guizhou Normal University, Guiyang, 550001, P. R. China
[§]State Key Laboratory of Physical Chemistry of Solid Surfaces, Xiamen University, Xiamen 361005, P. R. China

Supporting Information

ABSTRACT: The layer-by-layer growth of a surface-attached metal–organic framework (SURMOF), $[Cu_2(F_4bdc)_2(dabco)]$ (F_4bdc = tetrafluorobenzene-1,4-dicarboxylate and dabco = 1,4-diazabicyclo-[2.2.2]octane), on carboxylate- and pyridine-terminated surfaces has been investigated by various surface characterization techniques. Particular attention was paid to the dependency of the crystal orientation and morphology on surface functionality, deposition temperature, and first layer order. For the fully oriented deposition of SURMOFs, not only a suitable surface chemistry but also the appropriate temperature has to be chosen. In the case of carboxylate-terminated surfaces, the expected [100] oriented $[Cu_2(F_4bdc)_2(dabco)]$ SURMOF can be achieved at low temperatures (5 °C). In contrast, the predicted [001] oriented SURMOF on pyridine-terminated surface was obtained only at high deposition temperatures (60 °C). Interestingly, we found that rearrangement processes in the very first layer determine the final orientation (distribution) of the growing crystals. These effects could be explained by a surprisingly hampered substitution at the apical position of the Cu_2-paddle wheel units, which requires significant thermal activation, as supported by quantum-chemical calculations.

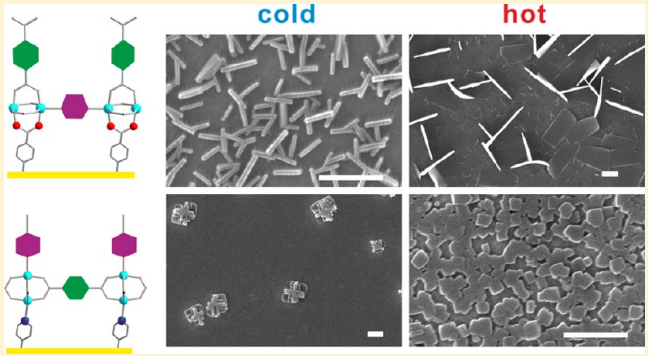

INTRODUCTION

The growth of metal–organic frameworks (MOFs) on surfaces gained significant attention due to the possibility not only to exert extraordinary control over the crystallographic orientation, the film thickness, or interdigitation but also to implement these films directly into devices, e.g., for sensorics.[1,2] Several methods have been developed to control the growth of such surface-attached MOFs (so-called SURMOFs) on various substrates.[3,4] Self-assembled monolayers (SAMs) turned out to be the most powerful tool for adjusting the surface chemistry of the substrates, since their headgroup chemistry can easily be adapted by synthetic means. It has been demonstrated by Wöll and co-workers that on SAM-functionalized surfaces a stepwise layer-by-layer (or liquid-phase epitaxial) growth of MOFs with a very high structural control is possible.[4a,b,5] By using a combination of *in situ* surface plasmon resonance (SPR) spectroscopy and quartz crystal microbalance (QCM) measurements these authors could also show that, in contrast to the hydrothermal approach, the layer-by-layer growth mechanism requires the employment of preformed metal clusters (such as the tetrakis-μ-carboxylatodi-copper unit) for a successful growth.[6] This led to a now generally accepted model for the origin of orientation of the SURMOF on either carboxylate-terminated or monodentate donor-terminated SAM surfaces (Figure 1, top).

Recent exceptions observed in particular for a series of tetragonal systems M_2L_2P (M = Cu, Zn; L = 1,4-benzenedicarboxylate (bdc), tetrafluorobenzene-1,4-dicarboxylate (F_4bdc), naphthalene-1,4-dicarboxylate (ndc); P = 1,4-diazabicyclo[2.2.2]octane (dabco), 4,4′-bipyridine (bipy), where the P ligands serve as pillar to connect the 2D M_2L_2 paddle wheel framework,[7] cf. Figure S1 (Supporting Information)) suggest, however, that the growth of SURMOFs might be more complicated than anticipated.[8] We therefore decided to investigate the influence of the chemistry in the very first layer on the morphology of the final multilayer SURMOFs. To this end we used infrared reflection absorption spectroscopy (IRRAS), which is a powerful tool for the determination of the structure and orientation even of ultrathin molecular layers.

Received: April 22, 2015
Published: June 8, 2015

DOI: 10.1021/jacs.5b03948
J. Am. Chem. Soc. 2015, 137, 8237–8243

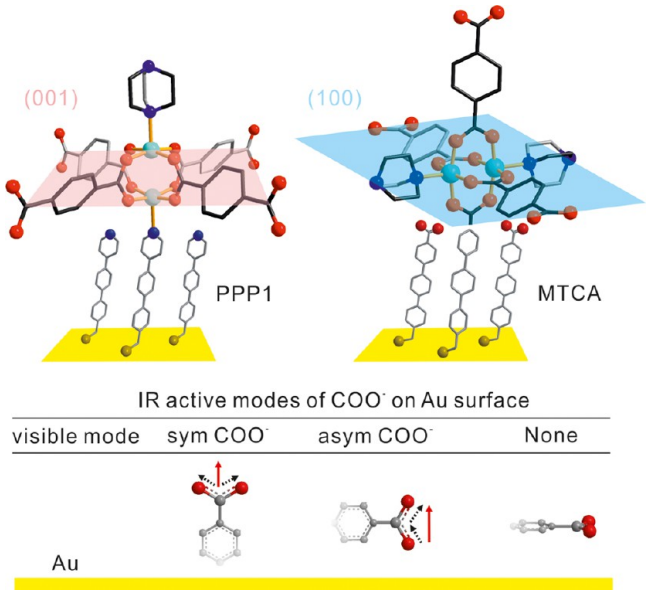

Figure 1. Top: The coordination of the tetrakis-μ-carboxylatodicopper unit onto surfaces terminated by a monodentate Lewis base (left, in form of a pyridine-terminated SAM) and carboxylate-terminated surfaces (right) is expected to influence the orientation of the resulting SURMOF, as indicated by the respective crystallographic planes. An expanded model is shown in Figure S1 (Supporting Information). Bottom: The surface selection rule permits the distinction of the three possible orientations of a carboxylate group by the appearance of the $-COO^-$ stretching bands in the IRRA spectra. The red arrows signify the transition dipole moments for the respective vibrational modes (black arrows).

RESULTS AND DISCUSSION

To obtain reproducible results, appropriate SAMs as well as a suitable SURMOF system had to be chosen. We used two SAMs of very high structural quality: The COOH-terminated SAM was formed from 4′-(mercaptomethyl)terphenyl-4-carboxylic acid (MTCA),[9] and the monodentate Lewis-base terminated one was formed from (4-(4-(4-pyridyl)phenyl)phenyl)methanethiol (PPP1).[10] As a SURMOF model we used $[Cu_2(F_4bdc)_2(dabco)]$,[11] a very compact system with a low degree of conformational freedom. The F_4bdc ligand was employed as dicarboxylate ligand, since it has a high symmetry (D_{2h}), does not show C−H vibrations interfering with those of other materials used during the preparation (dabco, starting materials, solvents), and—above all—shows shifted carboxylate vibrational energies compared to the acetate groups of the copper(II)acetate ($Cu_2(OAc)_4{\cdot}2H_2O$) precursor. Generally, the combination of the two carboxylate vibrational modes (asymmetric/symmetric stretching) with the selection rules in the vicinity of metallic surfaces[12] permits the exact determination of the orientation of the carboxylate groups, and thus of the tetragonal network, with respect to the surface (Figure 1, bottom). Thus, the IRRA spectrum of a tetrakis-μ-carboxylatodicopper unit should only show the signal of the asymmetric vibration at about 1670 cm^{-1} when its Cu−Cu axis is oriented parallel to the surface normal (corresponding to a [001] orientation of the crystalline bulk, see Figures 1 and S1 in the Supporting Information). The IRRA spectrum of the same complex exclusively exhibits the signal of the symmetric vibration at about 1410 cm^{-1} if the axis is oriented parallel to the surface ([100]/[010] orientation of crystals). This is in fact the case for the SURMOFs deposited on PPP1 and MTCA SAMs, respectively, under optimized conditions (Figure 2a).

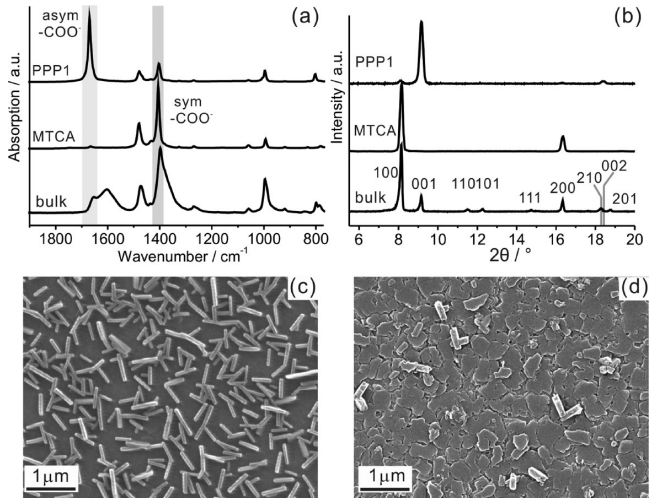

Figure 2. Oriented layer-by-layer growth of the $[Cu_2(F_4bdc)_2(dabco)]$ SURMOF on two different SAMs (PPP1 and MTCA). The orientation of the frameworks can be deduced by the presence/absence of the signals of the symmetric or asymmetric carboxylate vibrational bands in the IRRA spectra (a), of the respective reflections in the SXRD (b, background-corrected), and also from SEM images (c, d). These SURMOFs were grown on MTCA SAMs at 5 °C (c, 35 cy, see text for explanation) and PPP1 SAMs at 60 °C (d, 50 cy).

In line with the surface selection rule, the signals of the symmetric vibration of the carboxylate group (in the case of the deposit on PPP1) or the asymmetric vibration (the MTCA case) almost completely disappeared. Surface X-ray diffraction (SXRD, Figure 2b) confirms that this is in fact due to the preferential orientation of the crystals. The residual signals stem from very few misoriented crystals on the surfaces identifiable by scanning electron microscopy (SEM, Figure 2d). The in-plane XRD data (Figure S2 in the Supporting Information) further indicate that the SURMOF indeed has the same structure as observed for the bulk material. The central observation here is that this highly oriented growth occurs only at the temperatures indicated in the caption of Figure 2, that is, 60 °C for the PPP1-based system and 5 °C for the MTCA-based one (these temperatures are currently the extrema reachable in our experimental setup).

We figured that the temperature dependence can be used to understand the processes guiding the orientational distribution in the final systems. To find out whether the orientation of the SURMOFs is already predetermined in the very first layer as a function of the deposition temperature, we recorded IRRA spectra after each deposition step. From here on, we use the following nomenclature: “Full cycles” consisted of first dipping the substrates into the metal precursor solution (1 mM $Cu_2(OAc)_4{\cdot}2H_2O$ in ethanol), followed by a rinsing step, immersion into the ligand solution (0.1 mM H_2F_4bdc/0.1 mM dabco in ethanol), and another rinsing step. We refer to “half cycles” (0.5 cy) when the surfaces were immersed only in $Cu_2(OAc)_4$ solution and then rinsed. Since DFT calculations suggested that the symmetric carboxylate vibration in $Cu_2(OAc)_4$ coincides with a combination vibration of the $-CH_3$ groups (see Supporting Information, bands 5 and 6 in Figure S3 and Table S1), we used perdeuterated copper(II)acetate ($Cu_2(CD_3COO)_4{\cdot}2D_2O$, $Cu_2(OAc)_4$-d_{12}) in most experiments. Figure 3 depicts representative spectra taken on MTCA and PPP1 surfaces after 0.5 cycle and 1 cycle at different temperatures.

DOI: 10.1021/jacs.5b03948
J. Am. Chem. Soc. 2015, 137, 8237−8243

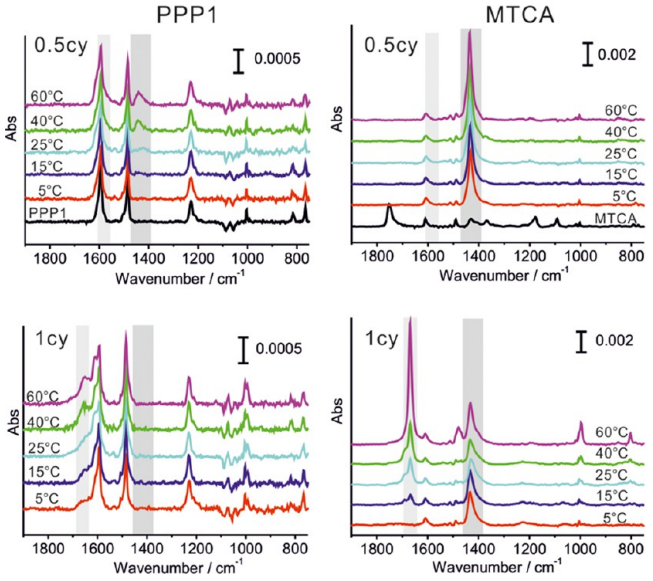

Figure 3. IRRA spectra of the deposits after immersion only in copper acetate solution (0.5 cy) and copper acetate solution followed by the ligand solution (1 cy). For comparison, the IRRA spectra of the pristine SAMs are given in the upper two graphs (black lines). The gray rectangles signify the areas where the carboxylate bands are expected to be found (light gray, asymmetric; dark gray, symmetric vibration), see text for explanation.

A number of interesting observations resulted from these series. It becomes immediately obvious that after 0.5 cycle the intensity of the signal of the symmetric vibration of the $-CO_2^-$ group (1440 cm^{-1}) in the MTCA case is independent of the deposition temperature, while on the PPP1 surface carboxylate signals appear only from samples deposited at 25 °C or higher. We verified by total external reflection X-ray fluorescence (TXRF) measurements (see Figure S6, Supporting Information) that these intensities in fact correspond to different surface coverages and not to chemical changes. These findings indicate surprisingly hampered substitution processes at the apical positions of the copper dimer, which are typically occupied by solvent molecules (in our case: water or ethanol). In contrast, substitution of the bidentate carboxylate ligand seems to proceed rapidly. This is in line with previous reports on QCM results for the *in situ* observation of the layer-by-layer deposition.[8,13]

The IRRA spectra give information not only about coverage but also about the orientation of the units. On the MTCA SAM, the complete invisibility of the asymmetric acetate carboxylate vibrational mode (expected at 1585 cm^{-1}) after 0.5 cycle indicates a perfect orientation of the Cu−Cu axes perpendicular to the surface normal at any deposition temperature. In contrast, at the PPP1 surface the orientation of the copper paddle wheels seems to be significantly less defined. The exact evaluation of the apparent tilt angle is hampered by the pyridine ring vibration (ν CC) at 1595 cm^{-1} superposed on the signal at 1585 cm^{-1}. After subtraction of the SAM spectra to minimize this interference (see Supporting Information, Figure S7), an upper limit for the tilt angle can be estimated using the Debe method on the relative intensities of the asymmetric and the symmetric $-CO_2^-$ bands.[14] In all cases, values around 50° result, which can only partially be explained by the tilt angle of the pyridine-terminated thiolates within the SAM (15−20°).[10] It must therefore be assumed that this unit experiences a significant degree of orientational freedom on the surface (as could be described, e.g., by a wagging mode). Note that a similar wagging of the $Cu_2(OAc)_3$ unit at the carboxylate-terminated surface does not lead to a change in the orientation of the Cu−Cu axis and thus cannot be detected by IRRAS.

Surprisingly, the situation changes drastically after introduction of the MOF ligands, completing the first cycle. On the PPP1 SAM, a perfect alignment of the Cu−Cu axis parallel to the surface normal can be achieved at any temperature, as indicated by the absence of the signal for the symmetric $-CO_2^-$ vibration (expected at 1410 cm^{-1}). Obviously, the F_4bdc ligands act as spreader bars forcing the upright orientation of the inorganic units. To fit these spreader bars perfectly in between the Cu_2 units, the latter must have some lateral mobility, e.g., by moving

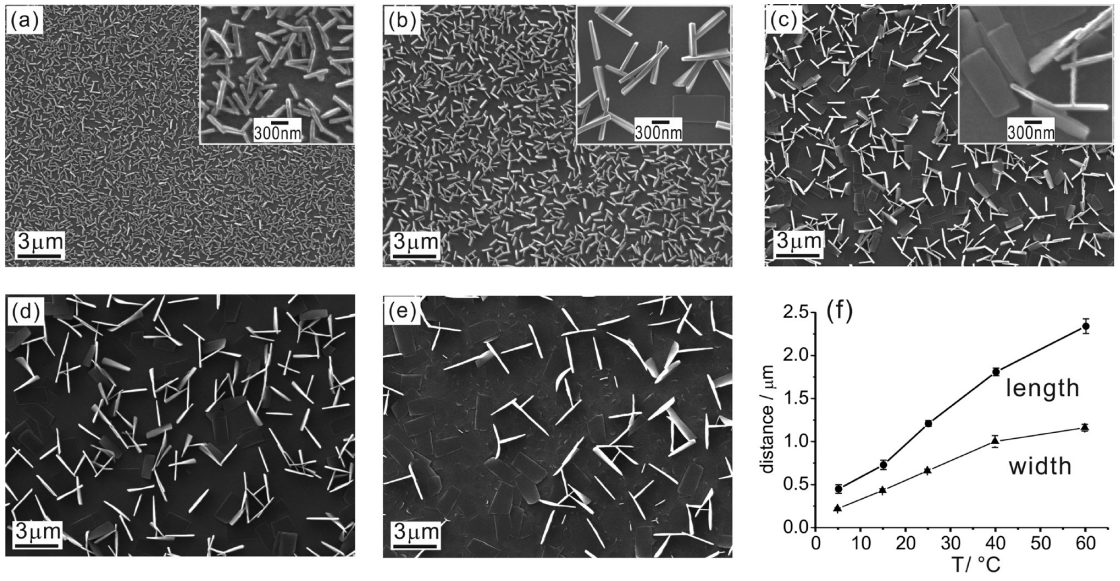

Figure 4. SEM images of $[Cu_2(F_4bdc)_2(dabco)]$ grown for 35 cycles on MTCA SAMs at various temperatures: (a) 5 °C; (b) 15 °C; (c) 25 °C; (d) 40 °C; (e) 60 °C. (f) Plot of length and width of the $[Cu_2(F_4bdc)_2(dabco)]$ crystals as a function of deposition temperature.

DOI: 10.1021/jacs.5b03948
J. Am. Chem. Soc. 2015, 137, 8237−8243

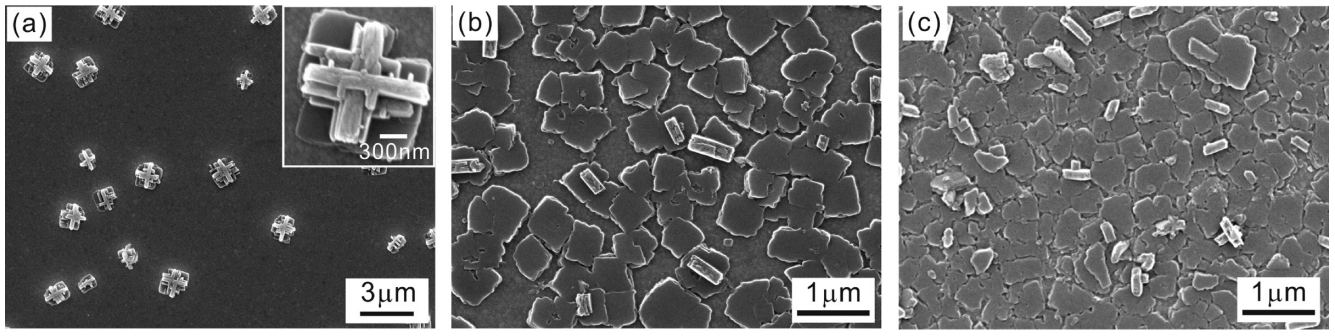

Figure 5. SEM images of $[Cu_2(F_4bdc)_2(dabco)]$ grown on PPP1 surface at various temperatures after 50 cycles: (a) 25 °C; (b) 40 °C; (c) 60 °C.

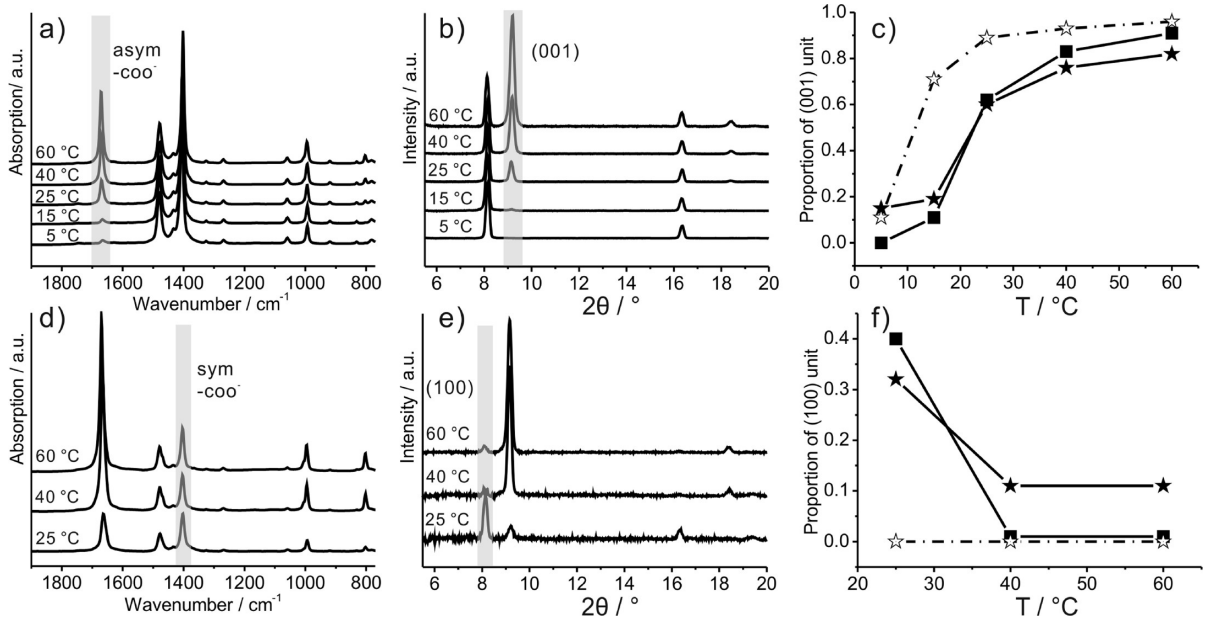

Figure 6. Temperature dependency of the orientation of the SURMOFs grown on MTCA (top) and PPP1 (bottom). From left to right are shown the IRRAS, SXRD (background-corrected), and orientational composition (filled squares, SXRD data; filled stars, IRRAS data of multilayer systems; open stars, IRRAS data of system after 1 cy). The spectra in panel a are normalized to the signal of the sym. $-CO_2^-$ vibration, and the diffractograms in panel b are normalized to the (100) peak. The value of 0 in panels c and f corresponds the orientations expected according to the model depicted in Figure 1. See text for explanation.

from one coordination site to the next. This assumption is supported by a recent observation of Anderson and co-workers, who found that the growth of another MOF based on the Cu_2 paddle wheel motive (HKUST-1) can be best described by the Volmer−Weber mechanism, which is based on such a lateral mobility.[15]

The picture is more complex for the MTCA surface: Here the perpendicular orientation of the Cu−Cu axis is maintained only at 15 °C and below, indicating a thermally activated reorientation process. The spectra clearly demonstrate that the acetate ligands (1440 and 1585 cm^{-1}) became exchanged by F_4bdc, the carboxylate vibrations of which appear at 1410 and 1670 cm^{-1}, respectively (see lines in Figure S7 in the Supporting Information). Their relative intensities suggest that at elevated deposition temperatures coordination networks are formed with a significant fraction of the copper dimers standing upright at the MTCA surface causing substantial orientational heterogeneity in the system.

We simulated a putative reorientation path of the Cu_2-carboxylate unit by quantum-chemical means with a minimalistic molecular model, employing trifluoroacetate (TFA) residues instead of F_4bdc linkers and methanol instead of ethanol molecules (see Supporting Information for details). For the resulting single cluster unit we obtain an energetically feasible reorientation mechanism, which involves a change from the bridging μ-η^1,η^1 coordination of the surface-bound carboxylate to a η^2-coordination mode induced by an incoming TFA ligand with concomitant saturation of the liberated Cu coordination site by dabco (see Supporting Information for details, Figure S8). The computed energy regime governing this reorientation process is in line with a thermally induced tilt of the Cu−Cu axis, as evidenced by the spectroscopic observations.

To test whether the orientational order of the respective first layers (1 cy) determines the orientation of the final SURMOFs, the growth was continued at the same temperatures for several cycles, until crystals could be observed by SEM and clean SXRDs could be obtained (35 cycles on MTCA and 50 cycles on PPP1, see Figures 4, 5, and 6).

On the MTCA surface, the layer-by-layer growth resulted in densely packed layers of rectangular, platelike crystals regardless of the deposition temperature. Nevertheless, the temperature had a remarkable influence on both the size of the MOF crystals and the orientation distribution. As depicted in Figure 4f, the size of the crystals in two dimensions (length/width) increases basically

DOI: 10.1021/jacs.5b03948
J. Am. Chem. Soc. 2015, 137, 8237−8243

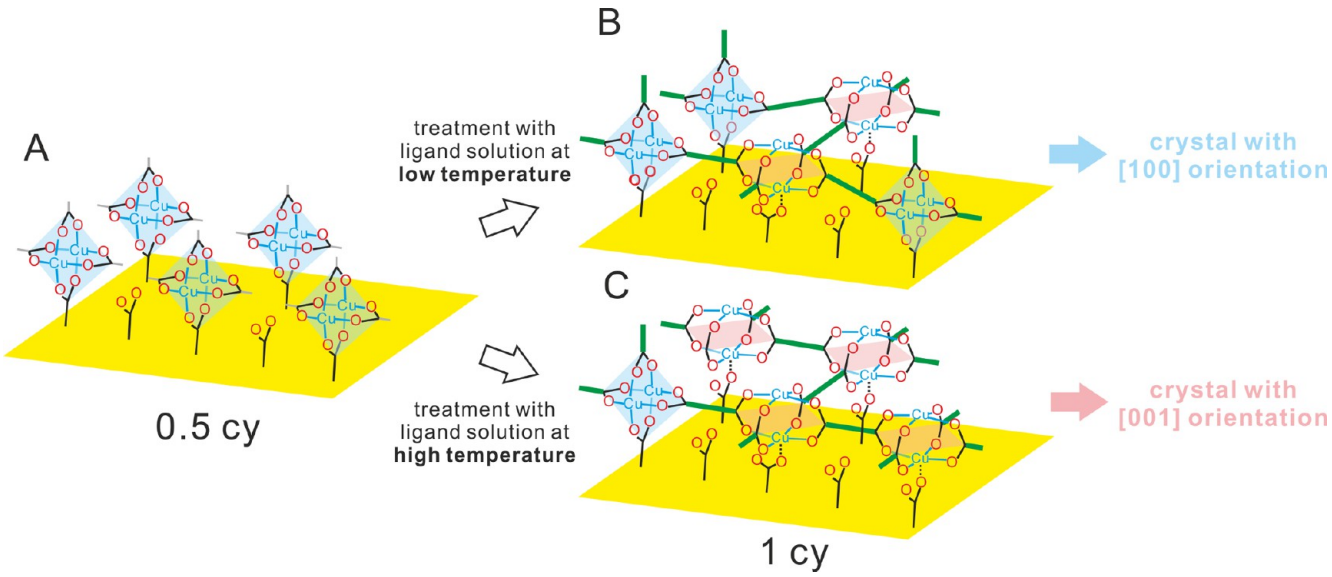

Figure 7. Model for the temperature dependent processes at a nucleus on the carboxylate-terminated surface (A) during the insertion of the dicarboxylate ligands (= green bold lines; the dabco ligands have been omitted for clarity). The mismatch between the coordination sites of the SAM and the MOF structure results in structural stress and disorder (B). At higher temperatures the stress becomes relaxed by a thermally activated reorientation of the Cu_2 units, which are then coordinated by the SAM-carboxyl groups at their apical site (C). The relative amount of reoriented units (pink) in the crystal nucleus at the MTCA surface must exceed a certain threshold to initiate the growth of crystals with the undesired [001] orientation. A similar situation occurs at the edges of the growing [001] oriented crystals on PPP1 surfaces.

linearly with the temperature while maintaining a ratio of about two. The third dimension, the thickness, is almost constant at all temperatures and amounts to about 80 nm after 35 cycles. Such an anisotropic growth has also been observed for other nanoporous materials, for which several growth mechanisms were proposed, such as birth-and-spread growth, spiral growth, and modulation growth mechanism.[16d] Our case presumably is best described by the birth-and-spread mechanism. As stated before, the deposition temperature influences not only the size of the MOF crystals but also their orientational distribution: While at low temperatures (5 and 15 °C), the nanoplates on MTCA surfaces show a highly uniform vertical alignment, the number of flat-lying plates increases dramatically with increasing deposition temperature. Note that in any case only these two orientations can be found, so no randomly tilted crystals were observed on the MTCA surfaces.

The situation on the PPP1 surface is entirely different. Here, the surface coverage by the MOF crystals depends significantly on the deposition temperature (Figure 5). Below 25 °C almost no crystals grow on this surface, while at 60 °C, full coverage is obtained. These observations are in accord with the results of the IRRAS as well as the TXRF measurements of the initial layer of these SURMOFs. Another significant difference is the relative amount and the growth mode of the vertically grown crystals. While, on the MTCA surface, crystals with both kinds of orientation grow from the SAM surface, on PPP1 the upright crystals always grow on top of flat-lying ones. This twinning of the crystals becomes particularly clear for the samples grown at 25 °C exposing a low crystal density: Obviously the misorientation does not result from defects in the monolayer but from some defect mechanism during crystal growth. These defects become repeated at the misoriented crystals (see the tiny protrusions at the side of the "upright" crystal part in the inset in Figure 5a), so that obviously a very general mechanism for their formation exists.

In order to quantify the effect of the deposition temperature on the crystal orientation, the samples were investigated using SXRD and IRRAS. The out-of-plane SXRD patterns of SURMOFs grown on MTCA at low temperatures (5 and 15 °C) exclusively show the (100) and (200) diffraction peaks ($2\theta = 8.15°$ and 16.3°, respectively, see Figure 6b). This indicates highly oriented growth along the [100] direction, consistent with the vast predominance of vertically aligned crystals as displayed in Figures 4a and 4b. The SXRD patterns of SURMOFs grown at higher deposition temperatures (25 to 60 °C) additionally exhibit (001) and (002) peaks ($2\theta = 9.15°$ and 18.3°, respectively) which are due to increasing fractions of flat-lying crystals (see Figures 4c–e). In the IRRA spectra, asymmetric $-COO^-$ stretch signals are present in the samples formed at deposition temperatures of 25 °C and higher. Their intensities rise with temperature, again indicating an increase of the number of flat-lying crystals, the crystallographic orientation of which allows for detection of this vibrational mode (Figure 6a).

The SXRD patterns (Figure 6e) of SURMOFs grown on PPP1 surfaces at high temperatures (40 and 60 °C) show predominant (001) and (002) diffraction peaks (9.15°, 18.3°) along with (100) signals of very low intensity. The latter become dominant at decreased deposition temperature (25 °C). This is accompanied by a low overall intensity of this diffraction pattern as a result of low surface coverage (note that, below 25 °C, no substantial growth of SURMOF crystallites on PPP1 surface could be observed at all). We infer from the diffraction data that high temperatures promote SURMOF growth on PPP1 surfaces along the [001] direction, which is in accord with the SEM results (*vide supra*). The ratio of the asymmetric and the symmetric $-COO^-$ stretch modes in the IRRAS data (Figure 6d) markedly increases with deposition temperature, also pointing to a predominant [001] orientiaton of the SURMOF crystals. Interestingly, even for high temperatures, the symmetric $-COO^-$ stretch signal is present, indicating a tendency of the SURMOF crystallites for twinning at all temperatures. Note that, in contrast to this, the

DOI: 10.1021/jacs.5b03948
J. Am. Chem. Soc. 2015, 137, 8237–8243

IRRAS data of the initial layer (1 cy) on PPP1 surface do not suggest the presence of any temperature-dependent orientational defects. We thus wanted to understand under which conditions the formation of such orientational defects occur.

For this, SXRD and IRRAS can be used to quantify the ratio between crystals with [100] and [001] orientation, since the crystallographic orientation is unambiguously connected to the orientation of the Cu_2 units. The proportions of crystals with the desired orientation can be calculated from the intensities of the respective signals (for the procedures see Supporting Information) and are depicted in Figure 6 (third column, filled symbols). As can be seen, the two methods produce very similar results, validating each other. Applying the same evaluation procedure to the IRRAS data obtained after 1 cy (Figure 3, bottom row) produces curves showing similar trends but significant differences (Figures 6c and 6f, open stars). On PPP1 SAMs, the high order within the first SURMOF layer (no [100] oriented material is found) can only be maintained in the multilayer systems at high deposition temperatures, with already significant misorientation at 25 °C (Figure 6f). Note that below this temperature—in line with the observations made at 0.5 cy—almost no SURMOF was formed, so that no data points could be obtained. On the MTCA surface, the orientational (dis-)order of the first layer (1 cy) becomes well communicated into the multilayer SURMOF system, with the best ordered systems (almost no [001] oriented crystals) formed at 5 °C (Figure 6c). Nevertheless, between 5 and 40 °C the orientational order of the crystals significantly exceeds that in the first layer, suggesting the existence of an ordering mechanism: On the MTCA surface the initially (after 0.5 cy) well-oriented Cu_2 units become orientationally disordered by the cross-linking via the bifunctional F_4bdc unit due to a mismatch between the MOF lattice and the SAM lattice (Figure 7). Based on the observation that at room temperature and below the substitution at the apical position of the Cu_2 unit seems to be significantly hampered compared to the substitution of the carboxylate ligands (*vide ultra*), we suggest that at low temperature the majority of the molecules keep their orientation despite the fact that some stress/disorder occurs in the MOF network, which can only be compensated in part by a conformational rearrangement of the SAM (Figure 7B). At higher temperatures, the system can increasingly relax by permitting more of the Cu_2 units to reorient, since the occupation of the apical position by a MTCA carboxyl group (pink units in Figure 7) becomes energetically feasible as demonstrated by the DFT calculations. Note that the coordination of the Cu_2 dimer at the apical position by additional carboxylate ligands has already been reported in the literature.[17] Such a partial reorientation also explains how the system still might be able to grow a majority of the desired, [100] oriented crystals: Each nucleus at the surface contains a certain ratio of misoriented to well-oriented Cu_2 units. Below a certain threshold, a crystal with the desired [100] orientation will grow; above this threshold, a [001] oriented crystal results.

This assumption is also confirmed by the scanning electron micrographs (Figure 4). On MTCA, all crystals, regardless of their orientation, directly grow from the substrate, meaning that their nuclei also have been located at the substrate. The situation is quite different for the disordered systems at PPP1, since here a reorientation of the Cu_2 units is not possible at the surface, resulting in their perfect orientation within the nuclei. In this case, disorder arises on top of the already grown, [001] oriented crystals by more or less pronounced twinning. The geometry of the twinning (centered, interpenetrated) suggests a flipping of

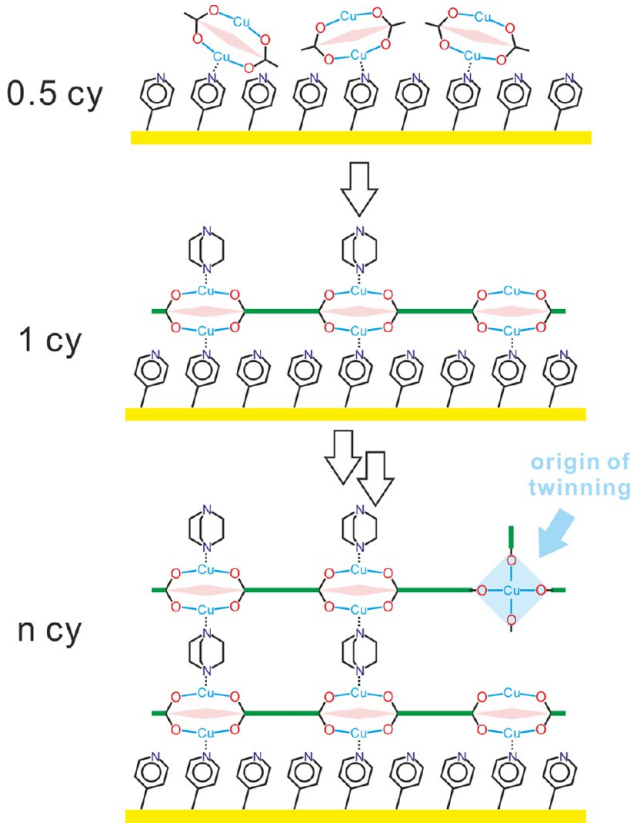

Figure 8. Model for the processes occurring during the layer-by-layer deposition at the monodentate donor-terminated PPP1 surface. The Cu_2 clusters deposited in the first half-cycle (0.5 cy) are orientationally disordered but become confined by addition of the bidentate F_4bdc (thick green lines). Due to the hampered substitution in the apical position, some of the Cu_2 units in the upper layers become not locked in place by the dabco bridges and therefore can rotate around the σ-bonds of the F_4bdc ligand. These units can act as twinning sites during the growth of the originally [001] oriented crystals.

some of the Cu_2 units during crystal growth (see Figure 8). Obviously, at temperatures of 25 °C and below, the energy of the system is too low to achieve the substitution at the apical coordination site, which would force all the Cu_2 cages into the correct orientation.

To demonstrate that this behavior is not specific for the presented system, and not even for the Cu_2 paddle wheel motif, we investigated the temperature dependent deposition of $[Zn_2(adc)_2(dabco)]$ with adc being 9,10-anthracenedicarboxylate. It is well established that the chemistries of the Zn and the Cu paddle wheels are quite distinct so that with these two systems a relatively wide range of systems is embraced.[18] As can be seen in the AFM images as well as the IRRA spectra (Figure S10 in the Supporting Information), very similar data can be obtained for this system, suggesting that the temperature dependency is a general phenomenon.

CONCLUSION

In conclusion, the layer-by-layer growth mechanism of tetragonal MOF systems grown on SAM functionalized surfaces is determined not only by the surface chemistry of SAMs but also by the surprisingly inhibited substitution reaction at the apical position of the paddle wheel metal cluster. Only when the deposition temperature is chosen adequately is the correct substitution pattern (apical vs equatorial) maintained/obtained

DOI: 10.1021/jacs.5b03948
J. Am. Chem. Soc. 2015, 137, 8237−8243

at the SAM/MOF interface and/or the MOF surface. For example on the pyridine-terminated PPP1 surface, and presumably any other monodentate Lewis-base terminated surface, elevated temperatures are necessary to achieve deposition of the tetrakis-μ-carboxylatodimetal units in the first place, but also to force the correct alignment of these units in subsequent layers. To characterize the orientation of the paddle wheel units even in the very first layer, IRRA spectroscopy turned out to be a sensitive and versatile tool, which can be complemented by SXRD measurements in the multilayer regime. Thus, this study provides vital details on the interplay of several factors (surface chemistry, deposition temperature, and first layer order) for the layer-by-layer growth of SURMOFs, which will help to control the fabrication of SURMOFs for many applications.

■ ASSOCIATED CONTENT

Supporting Information

Experimental details, DFT calculations, band assignment of IR spectra, TXRF data, quantum-chemical studies of the reorientation path, and evaluation procedure of the orientational composition of the SURMOFs. The Supporting Information is available free of charge on the ACS Publications website at DOI: 10.1021/jacs.5b03948.

■ AUTHOR INFORMATION

Corresponding Author

*aterfort@chemie.uni-frankfurt.de

Notes

The authors declare no competing financial interest.

■ ACKNOWLEDGMENTS

This manuscript is dedicated to the memory of Robert Heide. Financial support by the Beilstein-Institut, Frankfurt/Main, Germany within the research collaboration NanoBiC, the SKL of Xiamen University of China (No. 201413), and the National Natural Science Foundation of China (No. 21403040) are gratefully acknowledged. We thank Zhigang Gu, KIT, Germany, for recording the in-plane XRD.

■ REFERENCES

(1) (a) Meek, S. T.; Greathouse, J. A.; Allendorf, M. D. *Adv. Mater.* **2011**, *23*, 249−267. (b) Lu, G.; Hupp, J. T. *J. Am. Chem. Soc.* **2010**, *132*, 7832−7833. (c) Uehara, H.; Diring, S.; Furukawa, S.; Kalay, Z.; Tsotsalas, M.; Nakahama, M.; Hirai, K.; Kondo, M.; Sakata, O.; Kitagawa, S. *J. Am. Chem. Soc.* **2011**, *133*, 11932−11935. (d) Li, Y. S.; Bux, H.; Feldhoff, A.; Li, G. L.; Shen, W. S.; Caro, J. *Adv. Mater.* **2010**, *22*, 3322−3326.

(2) (a) Zacher, D.; Shekhah, O.; Wöll, C.; Fischer, R. A. *Chem. Soc. Rev.* **2009**, *38*, 1418−1429. (b) Zacher, D.; Schmid, R.; Wöll, C.; Fischer, R. A. *Angew. Chem., Int. Ed.* **2011**, *50*, 176−199. (c) Carne, A.; Carbonell, C.; Imhar, I.; Maspoch, D. *Chem. Soc. Rev.* **2011**, *40*, 291−305. (d) Liu, B.; Tu, M.; Fischer, R. A. *Angew. Chem., Int. Ed.* **2013**, *52*, 3402−3405. (e) Tsotsalas, M.; Liu, J.; Tettmann, B.; Grosjean, S.; Shahnas, A.; Wang, Z.; Azucena, C.; Addicoat, M.; Heine, T.; Lahann, J.; Overhage, J.; Bräse, S.; Gliemann, H.; Wöll, C. *J. Am. Chem. Soc.* **2013**, *135*, 7438−7441.

(3) (a) Hermes, S.; Schröder, F.; Chelmowski, R.; Wöll, C.; Fischer, R. A. *J. Am. Chem. Soc.* **2005**, *127*, 13744−13745. (b) Biemmi, E.; Scherb, C.; Bein, T. *J. Am. Chem. Soc.* **2007**, *129*, 8054−8055. (c) Li, Y. S.; Liang, F. Y.; Bux, H.; Feldhoff, A.; Yang, W. S.; Caro, J. *Angew. Chem., Int. Ed.* **2010**, *49*, 548−551. (d) Ranjan, R.; Tsapatsis, M. *Chem. Mater.* **2009**, *21*, 4920−4924. (e) Horcajada, P.; Serre, C.; Grosso, D.; Boissiere, C.; Perruchas, S.; Sanchez, C.; Férey, G. *Adv. Mater.* **2009**, *21*, 1931−1935. (f) Ameloot, R.; Stappers, L.; Fransaer, J.; Alaerts, L.; Sels, B. F.; De Vos, D. E. *Chem. Mater.* **2009**, *21*, 2580−2582. (g) Li, M.; Dinca, M. *Chem. Sci.* **2014**, *5*, 107−111.

(4) (a) Shekhah, O.; Wang, H.; Paradinas, M.; Ocal, C.; Schüpbach, B.; Terfort, A.; Zacher, D.; Fischer, R. A.; Wöll, C. *Nat. Mater.* **2009**, *8*, 481−484. (b) Shekhah, O.; Wang, H.; Kowarik, S.; Schreiber, F.; Paulus, M.; Tolan, M.; Sternemann, C.; Evers, F.; Zacher, D.; Fischer, R. A.; Wöll, C. *J. Am. Chem. Soc.* **2007**, *129*, 15118−15119. (c) Schoedel, A.; Scherb, C.; Bein, T. *Angew. Chem., Int. Ed.* **2010**, *49*, 7225−7228. (d) Makiura, R.; Motoyama, S.; Umemura, Y.; Yamanaka, H.; Sakata, O.; Kitagawa, H. *Nat. Mater.* **2010**, *9*, 565−571. (e) Motoyama, S.; Makiura, R.; Sakata, O.; Kitagawa, H. *J. Am. Chem. Soc.* **2011**, *133*, 5640−5643. (f) Makiura, R.; Kitagawa, H. *Eur. J. Inorg. Chem.* **2010**, *24*, 3715−3724. (g) Zhuang, J. L.; Ceglarek, D.; Pethuraj, S.; Terfort, A. *Adv. Funct. Mater.* **2011**, *21*, 1442−1447.

(5) (a) Shekhah, O.; Liu, J.; Fischer, R. A.; Wöll, C. *Chem. Soc. Rev.* **2011**, *40*, 1081−1106. (b) Fischer, R. A.; Wöll, C. *Angew. Chem., Int. Ed.* **2009**, *48*, 6205−6208. (c) Arslan, H. K.; Shekhah, O.; Wieland, D. C. F.; Paulus, M.; Sternemann, C.; Schroer, M. A.; Tiemeyer, S.; Tolan, M.; Fischer, R. A.; Wöll, C. *J. Am. Chem. Soc.* **2011**, *133*, 8158−8168.

(6) Shekhah, O.; Wang, H.; Zacher, D.; Fischer, R. A.; Wöll, C. *Angew. Chem., Int. Ed.* **2009**, *48*, 5038−5041.

(7) (a) Furukawa, S.; Hirai, K.; Nakagawa, K.; Takashima, Y.; Matsuda, R.; Tsuruoka, T.; Kondo, M.; Haruki, R.; Tanaka, D.; Sakamoto, H.; Shimomura, S.; Sakata, O.; Kitagawa, S. *Angew. Chem., Int. Ed.* **2009**, *48*, 1766−1770. (b) Chun, H.; Dybtsev, D. N.; Kim, H.; Kim, K. *Chem.—Eur. J.* **2005**, *11*, 3521−3529. (c) Seo, J.; Bonneau, C.; Matsuda, R.; Takata, M.; Kitagawa, S. *J. Am. Chem. Soc.* **2011**, *133*, 9005−9013. (d) Seki, K.; Mori, W. *J. Phys. Chem. B* **2002**, *106*, 1380−1385. (e) Chen, B.; Liang, C.; Yang, J.; Contreras, D. S.; Clancy, Y. L.; Lobkovsky, E. B.; Yaghi, O. M.; Dai, S. *Angew. Chem., Int. Ed.* **2006**, *45*, 1390−1393. (f) Ma, B. Q.; Mulfort, K. L.; Hupp, J. T. *Inorg. Chem.* **2005**, *44*, 4912−4914.

(8) (a) Zacher, D.; Yusenko, K.; Betard, A.; Henke, S.; Molon, M.; Ladnorg, T.; Shekhah, O.; Schüpbach, B.; De los Arcos, T.; Meilikhov, M.; Winter, J.; Terfort, A.; Wöll, C.; Fischer, R. A. *Chem.—Eur. J.* **2011**, *17*, 1448−1455. (b) So, M. C.; Jin, S.; Son, H. J.; Wiederrecht, G. P.; Farha, O. K.; Hupp, J. T. *J. Am. Chem. Soc.* **2013**, *135*, 15698−15701. (c) Xu, G.; Otsubo, K.; Yamada, T.; Sakaida, S.; Kitagawa, H. *J. Am. Chem. Soc.* **2013**, *135*, 7438−7441.

(9) Himmel, H. J.; Terfort, A.; Wöll, C. *J. Am. Chem. Soc.* **1998**, *120*, 12069−12074.

(10) (a) Liu, J.; Schüpbach, B.; Bashir, A.; Shekhah, O.; Nefedov, A.; Kind, M.; Terfort, A.; Wöll, C. *Phys. Chem. Chem. Phys.* **2010**, *12*, 4459−4472. (b) Schüpbach, B.; Terfort, A. *Org. Biomol. Chem.* **2010**, *8*, 3552−3562.

(11) Kitaura, R.; Iwahori, F.; Matsuda, R.; Kitagawa, S.; Kubota, Y.; Takata, M.; Kobayashi, T. C. *Inorg. Chem.* **2004**, *43*, 6522−6524.

(12) Greenler, R. G. *J. Chem. Phys.* **1966**, *44*, 310−315.

(13) Stavila, V.; Volponi, J.; Katzenmeyer, A. M.; Dixon, M. C.; Allendorf, M. D. *Chem. Sci.* **2012**, *3*, 1531−1540.

(14) Debe, M. K. *J. Appl. Phys.* **1984**, *55*, 3354−3366.

(15) Ohnsorg, M. L.; Beaudoin, C. K.; Anderson, M. E. *Langmuir* **2015**, *31* (22), 6114−6121.

(16) (a) Shoaee, M.; Anderson, M. W.; Attfield, M. P. *Angew. Chem., Int. Ed.* **2008**, *47*, 8525−8528. (b) John, N. S.; Scherb, C.; Shoaee, M.; Anderson, M. W.; Attfield, M. P.; Bein, T. *Chem. Commun.* **2009**, 6294−6296. (c) Attfield, M. P.; Cubillas, P. *Dalton Trans.* **2012**, *41*, 3869−3878. (d) Tsuruoka, T.; Furukawa, S.; Takashima, Y.; Yoshida, K.; Isoda, S.; Kitagawa, S. *Angew. Chem., Int. Ed.* **2009**, *48*, 4739−4743. (e) Holden, M. A.; Cubillas, P.; Attfield, M. P.; Gebbie, J. T.; Anderson, M. W. *J. Am. Chem. Soc.* **2012**, *134*, 13066−13073.

(17) (a) Grasdalen, H. *Acta Chem. Scand.* **1971**, *25*, 1103−1113. (b) Rao, V. M.; Manohar, H. *Inorg. Chim. Acta* **1979**, *34*, L213−L214. (c) Funahashi, S.; Nishimoto, T.; Hioki, A.; Tanaka, M. *Inorg. Chem.* **1981**, *20*, 2648−2651. (d) Hioki, A.; Funahashi, S.; Tanaka, M. *Inorg. Chem.* **1986**, *25*, 2904−2907.

(18) (a) Tan, K.; Nijem, N.; Canepa, P.; Gong, Q.; Li, J.; Thonhauser, T.; Chabal, Y. J. *Chem. Mater.* **2012**, *24*, 3153−3167. (b) Bhunia, M. K.; Hughes, J. T.; Fettinger, J. C.; Navrotsky, A. *Langmuir* **2013**, *29*, 8140−8145.

DOI: 10.1021/jacs.5b03948
J. Am. Chem. Soc. 2015, 137, 8237−8243